Article

Enhancing Oil–Water Separation Efficiency with WO$_3$/MXene Composite Membrane

Abdelfattah Amari [1], Haitham Osman [1], Mohamed Boujelbene [2], Maha Khalid Abdulameer [3], Miklas Scholz [4,5,6,7,8,*] and Saad Sh. Sammen [9,*]

1. Department of Chemical Engineering, College of Engineering, King Khalid University, Abha 61411, Saudi Arabia; abdelfattah.amari@enig.rnu.tn (A.A.); haman@kku.edu.sa (H.O.)
2. Industrial Engineering Department, College of Engineering, University of Ha'il, Ha'il 81451, Saudi Arabia; mboujelbene@yahoo.fr
3. Department of Radiology & Sonar Technologies, Al-Noor University College, Nineveh 41012, Iraq; maha.khalid@alnoor.edu.iq
4. Department of Urban Drainage, Bau & Service Oberursel (BSO), Postfach 1280, 61402 Oberursel (Taunus), Germany
5. Department of Civil Engineering Science, School of Civil Engineering and the Built Environment, Faculty of Engineering and the Built Environment, University of Johannesburg, Kingsway Campus, Aukland Park 2006, P.O. Box 524, Johannesburg 2092, South Africa
6. Kunststoff-Technik Adams, Specialist Company According to Water Law, Schulstraße 7, 26931 Elsfleth, Germany
7. Nexus by Sweden, Skepparbacken 5, 722 11 Västerås, Sweden
8. Department of Town Planning, Engineering Networks and Systems, South Ural State University (National Research University), 76, Lenin Prospekt, Chelyabinsk 454080, Russia
9. Department of Civil Engineering, College of Engineering, University of Diyala, Baqubah 32001, Iraq
* Correspondence: miklas.scholz@bso-oberursel.de or mscholz@uj.ac.za or miklas.scholz@kunststoff-technik-adams.de (M.S.); saad123engineer@yahoo.com (S.S.S.)

Abstract: In this study, a novel method for the high-performance treatment of oily wastewater was introduced using a tungsten (VI) oxide (WO$_3$)/MXene composite membrane based on poly (arylene ether sulfone) (PAES). Composite membranes were fabricated with superhydrophilic (SH) and superoleophobic (SO) characteristics, which allow for the high-performance treatment of oily wastewater. The fabricated composite membrane can also photodegrade organic types of pollutants with just a short period of UV, enabling self-cleaning and anti-fouling properties. Moreover, the comprehensive characterization of the composite membrane through FTIR, SEM, and XRD analyses yielded valuable insights. The FTIR analysis revealed the characteristic peaks of WO$_3$, MXene, PAES, and the synthesized composite membrane, providing essential information on the chemical composition and properties of the materials. The XRD results demonstrated the crystal structures of WO$_3$, MXene, PAES, and the synthesized composite membrane, further enhancing our understanding of the composite membrane. Additionally, the SEM images illustrated the surface and cross-section of the fabricated membranes, highlighting the differences in pore size and porosity between the PAES membrane and the WO$_3$–MXene composite membrane, which directly impact permeate flux. The study showed that the composite membrane had a remarkable recovery time of only 0.25 h, and the efficiency of the separation process and water flux recovered to 99.98% and 6.4 L/m^2.h, respectively. The joint influence of WO$_3$ and MXene on composite membranes degraded contaminants into non-polluting substances after sunlight irradiation. This process effectively solves the treatment performance and decrease in permeate flux caused by contamination. The technology is membrane-based filtration, which is a simple and advanced method for treating polluted water. This innovative work offers promising solutions to address water pollution challenges and holds potential for practical applications from a self-cleaning and anti-fouling point of view.

Keywords: oil–water separation; MXene composite membrane; superhydrophilic membrane; self-cleaning and anti-fouling membrane

1. Introduction

Water pollution, a growing global threat, jeopardizes human and ecological health. Wastewater contamination fouls rivers, nutrient imbalances harm coastlines, and climate change disrupts water and food supplies, all posing significant risks [1]. A key culprit is improper industrial wastewater disposal [2], as well as the use of agricultural poisons and their byproducts, which leads to surface water pollution [3]. Water quality, a multifaceted concept, depends on various intended uses. Water quality standards, a set of legal regulations, aim to prevent pollution and limit contaminant levels based on specific water uses [4]. Governments and aid organizations have made strides in recent years to provide clean water access to those in water-scarce regions [5].

Industrial activities often contribute to water pollution through leaks of organic solvents [6]. Traditional pollution treatment methods often face limitations, such as high costs, operational complexity, and environmental concerns. Energy-intensive methods may not be suitable for large-scale industrial applications [7]. Methods that require energy input are not suitable for large-scale industrial production [8]. However, membrane separation technology is a flexible, low-cost, and energy-efficient method that has been extensively applied to remove water pollution caused by oily wastewater. This technology has several advantages over other methods [9,10].

Membrane separation technology offers a promising solution to the limitations of conventional pollutant treatment methods, prompting ongoing research and development in this field [11,12]. However, a key challenge for this technology is membrane fouling, which reduces performance and increases costs. Fouling manifests in several ways: decreased water flow (flux), reduced pollutant rejection, and higher energy consumption.

Membrane fouling is a significant issue in the implementation of membrane separation technology. It can cause several problems, including a decline in the flux, rejection reduction, and high energy consumption. These issues can lead to increased operating costs. Membrane fouling can also reduce the permeate flux, permeate quality, and process performance. To mitigate fouling in membrane separation processes, various modification methods have been used. To address fouling, various membrane modification methods have been explored. One promising approach utilizes photocatalytic degradation self-cleaning composite membranes [13,14].

A recent innovation, self-cleaning polymer membranes are nanostructured materials with exciting potential across various applications [15]. These eco-friendly membranes, made from non-toxic polymers, can be processed into thin films that repel dirt, dust, and water. In other words, the secret lies in their surface chemistry. A layer of hydrophobic and oleophobic polymers repels water and oil, respectively [16]. These self-cleaning properties can be further enhanced by incorporating nanoparticles like titanium dioxide or zinc oxide. These nanoparticles improve the membranes' ability to repel contaminants and clean themselves, while also increasing their durability.

The applications for self-cleaning polymer membranes are extensive. They are valuable in industrial settings for food and medical packaging, and automotive parts [17]. Consumer products like cleaning cloths, solar cells, and other photovoltaic devices can also benefit from this technology [18]. Essentially, their self-cleaning nature makes them a compelling choice for a wide range of industrial and consumer applications [19].

Photocatalysis offers an eco-friendly and efficient approach to environmental preservation and new energy development, particularly for removing persistent organic pollutants [20]. However, limitations like fast charge recombination and low visible light utilization hinder its industrial application [21]. One promising strategy to overcome these limitations involves co-catalysts that modify the photocatalytic mechanism [22,23]. Researchers have also explored photocatalysts for wastewater treatment and the integration of these systems with membrane filtration.

MXene ($Ti_3C_2T_x$) is an emerging material that has gained attention in the photocatalysis field. It is a two-dimensional nanomaterial that can be constructed from different elements. MXene has a unique 2D layered structure, which provides a higher specific

surface area, more reaction sites, and good photocatalytic ability [24]. The wide spacing between the layers of $Ti_3C_2T_x$ allows ions to travel through the layers at high speed, while the hydroxyl or surface terminal groups of $Ti_3C_2T_x$ can provide sites with active photocatalytic reactions. Despite its promise, MXene faces challenges such as limited membrane-forming ability and poor stability. Recent research focuses on addressing these limitations through improved synthesis methods, characterization techniques, and surface modifications. Notably, functionalized MXenes with layer-dependent band gaps show enhanced photocatalytic performance [25]. Further research is needed to find the potential of MXene in photocatalysis and overcome its limitations to enable its widespread application in membrane materials.

Li et al. [26] provided research on self-cleaning materials with the potential for the treatment of oil in water. They synthesized a composite membrane using cross-linked tannic acid of polyvinyl alcohol (PVA–TA) and investigated the potentials of photocatalytic reactions by doping magnetic TiO_2 NPs and MXene. The surface of the composite membrane was constructed by $MTiO_2$, and the membrane showed SH/SO properties. It was claimed that the fabricated membranes had high efficiency in removing oil from water with a long life of service after 64 test cycles.

Lin et al. [27] conducted research on a two-dimensional (2D) $Bi_2O_2CO_3$@MXene membrane with photocatalytic properties and its abilities for the treatment of water. The composite membrane was synthesized using a simple method based on PVA–TA and N–doped $Bi_2O_2CO_3$ nanoparticles. The obtained data showed a high water flux of 815.3 $L \cdot m^{-2} \cdot h^{-1}$ and excellent oil–water separation performance (over 99%) for three different types of feeds. The membrane also demonstrated a high removal of dyes using adsorption and photochemical decomposition.

He et al. [28] focused on the development of a tungsten (VI) oxide (WO_3)/MXene composite membrane based on poly (arylene ether sulfone) (PAES) for efficient oil-in-water treatment. The paper highlights the SO and SH of the fabricated membrane, which enable the high-performance treatment of oil in water as the feed, and the photodegradation properties of the composite membrane, which can degrade the organic pollutants with just a small amount of sunlight irradiation, enabling self-cleaning.

Kusworo et al. [29] conducted a study on photocatalytic materials applied to wastewater removal by using a decomposition process followed by the membrane plant. They modified the PVDF membrane by applying WO_3 and MoS_2. The PVDF-MSW-PVA membrane showed a good performance in photodecomposition and a high capability of self-cleaning. This study suggests that the modified membrane can be used for wastewater removal by using a decomposition process followed by the membrane plant.

Our study presents an innovative and novel approach to efficiently treat oil-in-water mixtures using a tungsten (VI) oxide (WO_3)/MXene composite membrane based on poly (arylene ether sulfone) (PAES). This study introduces the first reported use of a WO_3/MXene composite membrane for efficient oil–water separation. The WO_3/MXene membrane has SH and SO features, which enable the high-performance treatment of oil in water as the feed. Additionally, the fabricated membrane can photodegrade organic pollutants with just a small amount of sunlight irradiation, enabling self-cleaning.

In other words, the primary objectives of this study are twofold: 1. Enhance the oil–water separation performance; 2. Investigate the self-cleaning and anti-fouling properties of the WO_3/MXene composite membrane under light irradiation. The novelty of our study lies in the unique combination of materials and their synergistic effects:

- WO_3/MXene composite: This is a novel approach for oil–water separation membranes. The existing research primarily focuses on pristine MXene membranes or composites with other materials.
- Enhanced separation efficiency: The introduction of WO_3 is expected to improve the membrane's underwater oleophobicity, leading to superior oil rejection compared to pristine MXene membranes.

- Photocatalytic self-cleaning: WO$_3$ possesses photocatalytic properties that can degrade organic contaminants under light irradiation. This could significantly improve the membrane's reusability and anti-fouling properties, addressing a major challenge for MXene membranes.

By combining these elements, our study explores a promising avenue for developing efficient, reusable, and self-cleaning oil–water separation membranes. This approach has the potential to overcome the limitations of existing methods and contribute to more sustainable water treatment solutions.

2. Materials and Methods

2.1. Materials

Tungsten (VI) oxide (WO$_3$) powder (99.99%) was purchased from Otto Chemie Pvt. Ltd. (Mumbai, India) Aqueous dispersions of single-layer Ti$_3$C$_2$T$_x$ (MXene) were obtained from Laizhou Kai Xi Ceramic Materials Co., Ltd. (Yantai, China). Block copolymer of poly (arylene ether sulfone) (PAES) was obtained by the method introduced by Harrison et al. [30]. Hydrochloric acid (37%w), sodium hydroxide, anhydrous lithium chloride, N–Methylpyrrolidone (NMP), and ethanol were purchased from Sigma-Aldrich (St. Louis, MO, USA). The gasoil, petrol, xylene, oil bean, oil gear, and aniline (AR grade) were obtained from Otto Chemie Pvt. Ltd.

2.2. Preparation of Composite Membrane

To prepare the WO$_3$–MXene composite membrane, poly (arylene ether sulfone) (PAES) (3 g) was dissolved in a 1:1 *v/v* mixture of N–methylpyrrolidone (NMP) and ethanol (80 mL) under magnetic stirring at 85 °C for 2 h. This step ensures the complete dissolution of the polymer and promotes the formation of a homogeneous casting solution. Subsequently, 0.9 g of tungsten (VI) oxide (WO$_3$) was added to the solution and stirred vigorously for 25 min. This step facilitates the uniform dispersion of WO$_3$ nanoparticles throughout the polymer matrix, which is crucial for achieving synergistic effects in the composite membrane. The temperature of the solution was then lowered to 65 °C to avoid the thermal degradation of MXene. Then, 3.5 mL of MXene dispersion was carefully added dropwise to the mixture and stirred continuously for an additional 30 min. This approach promotes the uniform distribution of MXene within the casting solution, maximizing their potential for efficient oil–water separation. The resulting well-mixed solution was cast onto a leveled glass plate and allowed to dry at 75 °C for 6 h. This initial drying step facilitates solvent evaporation and initiates membrane formation. Finally, the glass plate with the cast membrane was placed on top of a neodymium magnet and dried at 60 °C for 6 h. The magnetic field aids in aligning the MXene flakes within the membrane structure, potentially enhancing its separation performance. After drying, the composite membrane was carefully peeled off the glass plate for further characterization and performance evaluation.

The thickness of the fabricated WO$_3$/MXene composite membrane was measured using a micrometer at multiple points, and the average thickness was found to be 137 $\pm$ 2 μm.

By following this meticulous fabrication process, we aimed to achieve a WO$_3$/MXene composite membrane with a well-defined thickness, uniform distribution of components, and potentially enhanced performance for oil–water separation.

2.3. Instruments and Characterization

The samples were described for their functional groups by applying Fourier transform infrared spectroscopy (FTIR-7600, Lambda Scientific Pty Ltd., Edwardstown, Australia) with a 5 cm^{-1} scan rate and 4000–500 cm^{-1} scan range. X-ray diffractometry (XRD, EQUINOX 100, Thermo Fisher Scientific, Waltham, MA, USA) was applied to study the prepared samples with a scanning angle of 5–55° and 5° per min scanning speed. The obtained materials were also studied using X-ray photoelectron spectroscopy (XPS, Esclab 250 Xi, Thermo Fisher, Waltham, MA, USA). The wettability characteristics of the fabricated membranes, specifically their hydrophilicity (water-loving) and oleophobicity

(oil-repelling) nature, were evaluated. This technique involves placing a droplet of a specific liquid (e.g., deionized water or oil) onto the membrane surface using a micro-syringe. The goniometer then captures a high-resolution image of the droplet and the contact it forms with the membrane surface. The oleophobicity and hydrophilicity of the obtained materials were measured using the contact angle system (HZJC-3, Huazheng Electric Manufacturing, Baoding, China).

The contact angle (θ) is defined as the angle formed between the tangent line drawn at the liquid–vapor–solid interface (triple point) and the solid surface. A higher contact angle indicates a more hydrophobic surface, where the droplet sits on top with minimal interaction with the membrane. Conversely, a lower contact angle signifies a more hydrophilic surface, where the droplet spreads and wets the membrane more readily.

The obtained materials were optically investigated over 200–2500 nm by applying a UV–Vis spectrophotometer (METTLER TOLEDO, Greifensee, Switzerland), and SEM analysis was used to investigate the morphology of the synthesized membranes.

A CELSA500/350 Xenon lamp was used for simulated sunlight irradiation. An electrochemical analyzer was used to photoelectrochemically characterize the samples under a xenon lamp.

2.4. Oil-in-Water Filtration Test

The performance of a membrane in separating water–oil emulsions using a micro-filtration process was investigated. For this purpose, an emulsion of water–oil with a concentration of 5000 mg of oil per liter was evaluated as the feed. To prepare the feed, 80 Tween was used as an emulsifier to prepare a stable emulsion for feed production. The feed preparation method involved weighing the oil, which can be bean oil, petrol, gear oil, xylene, or aniline, to the desired amount, adding 200 L/mg of emulsifier to the water–oil solution, and using a high-speed mixer to prepare a stable emulsion. The mixing process was carried out for 10 min at a speed of 1200 revolutions per minute. A pump transferred the water–oil emulsion stored in a 5 L transparent plexiglass tank into the system. The pump's variable speed motor, controlled by a pressure sensor in the return flow path, maintained the required operating pressure of 3 bar. This controller adjusted the motor speed using a pressure sensor installed in the return flow path, regulating the motor speed to maintain the required operational pressure. The flow rate of the feed was also measured before entering the membrane module using a liquid flow meter calibrated for the desired feed. Additionally, two pressure sensors were used to measure the flow pressure before and after the membrane module, and the permeate flux rate was recorded using a digital scale.

The membrane module used was made of plexiglass and had dimensions of 215 × 165 mm. The membrane was prepared to the appropriate dimensions and was placed between these two plates. The feed was circulated in the system by a pump under operational conditions that were stabilized before each experiment. The process was such that the return flow was recycled back to the feed tank, and the amount of permeate passing through the membrane was measured using a digital scale and stored in a separate container. Prior to each experiment, the membranes were placed in a container containing distilled water for at least 24 h, and wet and swollen membranes were used in the performance test. Based on the trend of the flow rate over time in all experiments, the process time was set at 60 min for measuring the pure water flux and 60 min for the water–oil feed. Due to the low volume of permeate compared to the total feed volume and the return of its cycles to the feed tank, the water–oil feed concentration was assumed to be constant. After the end of the experiment, the system was emptied of the water–oil emulsion and washed with distilled water in the final stage to obtain water with a quality similar to distilled water.

The performance of the membrane in separating water–oil emulsions was determined by measuring the permeate flux rate through the membrane and the amount of oil retained in the product (the amount of oil remaining in the feed after passing through the membrane). After preparing the feed with a concentration of 5000 mg per liter of oil, the desired membrane was placed under operational conditions using distilled water for one hour.

This was to prevent unwanted and undesirable changes in membrane hydraulic resistance during the process. With the start of the experiment and the filtration of the main feed, the flow rate passing through the membrane was measured at predetermined time intervals. When the permeate flux rate reached a constant value, this value was recorded, and the flow rate sample was used for COD analysis.

The flow rate passing through the membrane at different times was calculated according to Equation (1).

$$J_w = \frac{V}{A.\Delta t} \tag{1}$$

where parameter V is equal to the volume of water passing through with a unit of liters, A is equal to the surface area of the membrane placed in the membrane module with a unit of m^2, and Δt is equal to the filtration time with a unit of hours. Finally, J_W is the water flow rate passing through the membrane with a unit of L/m^2 h.

The percentage of oil retention was calculated from Equation (2), in which Cf and Cp are the feed concentration and the permeate concentration, respectively.

$$\%R = \frac{(Cf - Cp)}{Cf} \times 100 \tag{2}$$

3. Results and Discussion

Characterization

Figure 1 presents the FTIR curves of the synthesized composite membrane, PAES, MXene, and WO$_3$. The FTIR spectra of WO$_3$ show the characteristic peaks that correspond to the vibrational modes of the tungsten–oxygen bonds. The exact position and intensity of these peaks depend on the synthesis method, particle size, and crystal structure of the WO$_3$ sample. Therefore, the FTIR spectrum of WO$_3$ can present valuable information on the chemical composition and properties of the material. The FTIR spectrum of the synthesized WO$_3$ and WO$_3$–Ag composites shows characteristic peaks at 600–900 cm^{-1}, which correspond to the stretching vibrations of the W–O bonds [31]. The FTIR spectrum of tungsten oxide thin films shows characteristic peaks at 1300–1600 cm^{-1}, which correspond to the W–O bonds [32]. The sites on the surface that show characteristic peaks at 3500–4000 cm^{-1} correspond to the W–O vibrations of stretching [33].
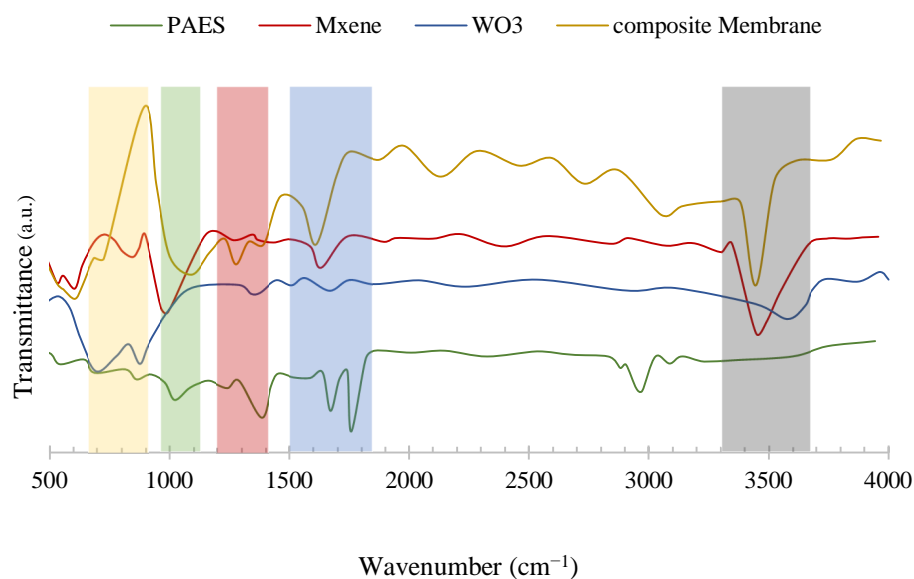

Figure 1. The FTIR curves of synthesized composite membrane, PAES, MXene, and WO$_3$.

The FTIR spectra of Ti$_3$C$_2$T$_x$ MXene show characteristic peaks that correspond to the vibrational modes of the Ti–C and Ti–O bonds. The exact position of the obtained peaks

depends on the synthesis method, particle size, and crystal structure of the $Ti_3C_2T_x$ MXene sample [34]. The obtained peaks in this study were observed in two different ranges: 600–1000 cm^{-1} and 3300–3700 cm^{-1}.

The FTIR spectra of PAES show characteristic peaks that correspond to the vibrational modes of the aryl ether and sulfone groups [35]. The peak at around 1500–1600 cm^{-1} corresponds to the aryl ring stretching vibration in the aryl ether group. The peak at around 1200–1300 cm^{-1} corresponds to the stretching vibration of the sulfone [36]. The peak at around 1000–1100 cm^{-1} is related to the C–O bond in the aryl ether group. The peak at around 700–800 cm^{-1} corresponds to the bending of the C–S bond in the sulfone group.

Figure 2 presents the XRD results of the synthesized composite membrane, PAES, MXene, and WO_3. The XRD pattern for the WO_3 samples shows characteristic peaks at around 23–25°, which correspond to the crystal structure. The XRD analysis of PAES shows characteristic peaks at around 15–25° and 25–35°, which correspond to the crystal structure. The intensity and position of these peaks depend on the degree of sulfonation, annealing temperature, and other factors. The peak at 10° in the XRD pattern of MXene is characteristic of the c–lattice parameter in MAX phases, which are the precursors of MXene. The position and intensity of this peak can provide information on the crystal structure and orientation of the MXene sample [37].
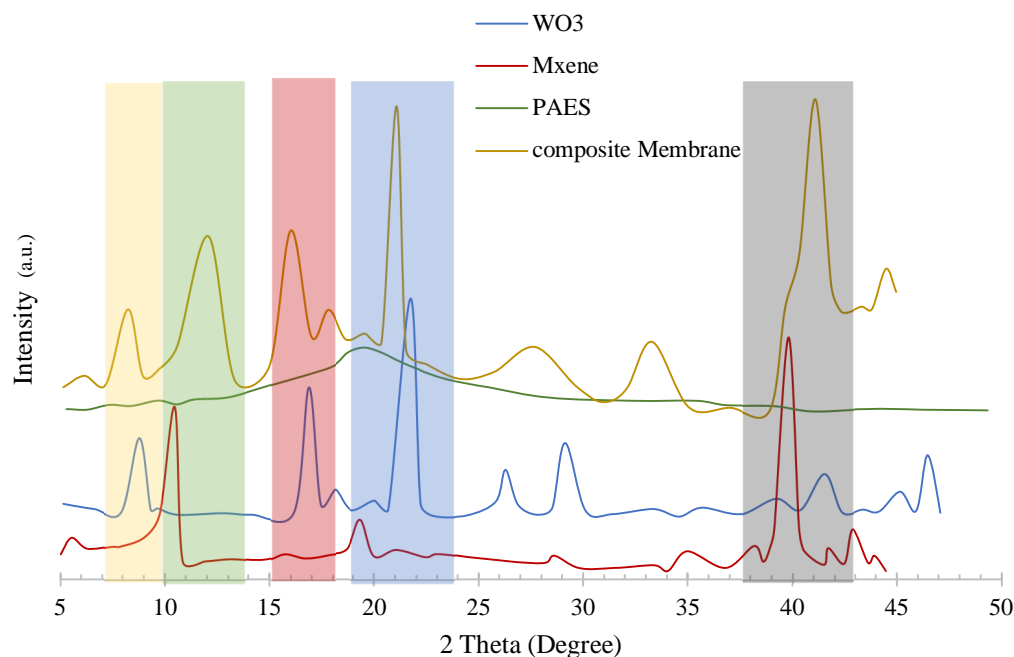

Figure 2. The X−ray diffraction (XRD) curves of the synthesized composite membrane, PAES, MXene, and WO_3.

The appearance of the 35–45° angle in the patterns of MXene films can arise from an amalgamation of the obtained material. This can affect the interpretation of the XRD data and the determination of the crystal structure of the material [38].

The XPS test was conducted to provide further confirmation of the MXene composition. As can be seen from Figure 3, the full spectrum of the materials reveals the existence of tungsten, Ti, O, and C elements. The 256.8 eV in the spectrum of C 1s corresponds to the C–C bond. The peak at 284.4 eV in the spectrum of C 1s corresponds to the C–Ti bond. The peaks at 528.5 eV and 561.8 eV in the spectrum of O 1s correspond to the C–O and C=O bonds. The peaks at 522.8 eV and 492.0 eV in the spectrum of O 1s are the MXene C–Ti–OHx and C–Ti–Ox bonds. The peaks at 458.0 eV and 493.5 eV in the Ti 2p spectra are Ti–O 2p3/2 and Ti–O 2p1/2.
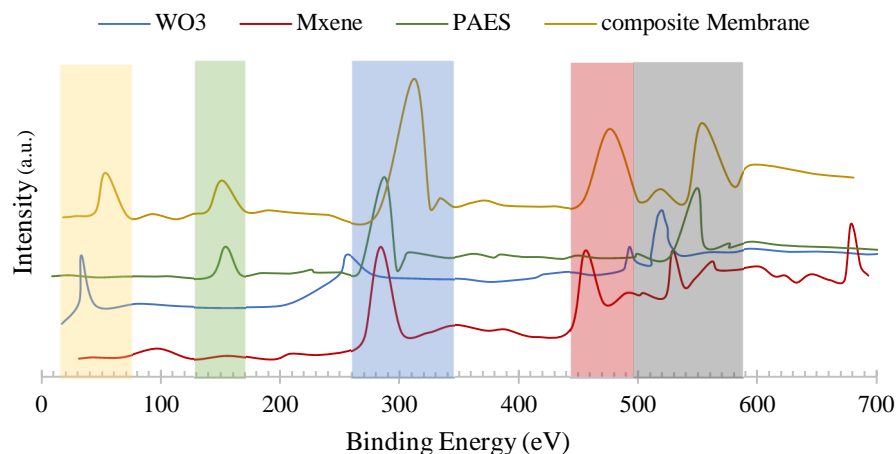
Figure 3. The XPS curves of synthesized composite membrane, PAES, MXene, and WO$_3$.

Figure 4 highlights the remarkable hydrophilic properties of the WO$_3$–MXene composite membrane, which demonstrated superwetting characteristics. The contact angle of a water droplet on the membrane decreased from $180° \pm 1°$ to $0° \pm 0.3°$ within a mere 0.25 s. This finding aligns with previous studies that have investigated the wettability of membranes based on MXene, where the addition of MXene material to the membrane has been shown to enhance hydrophilicity. The results of this study suggest that the WO$_3$–MXene composite membrane holds great potential for oil–water separation applications due to its superwetting properties. In other words, the membrane's ability to rapidly change its contact angle and its consistency with other MXene−based membrane studies highlight its promise in addressing the challenge of efficient oil–water separation.
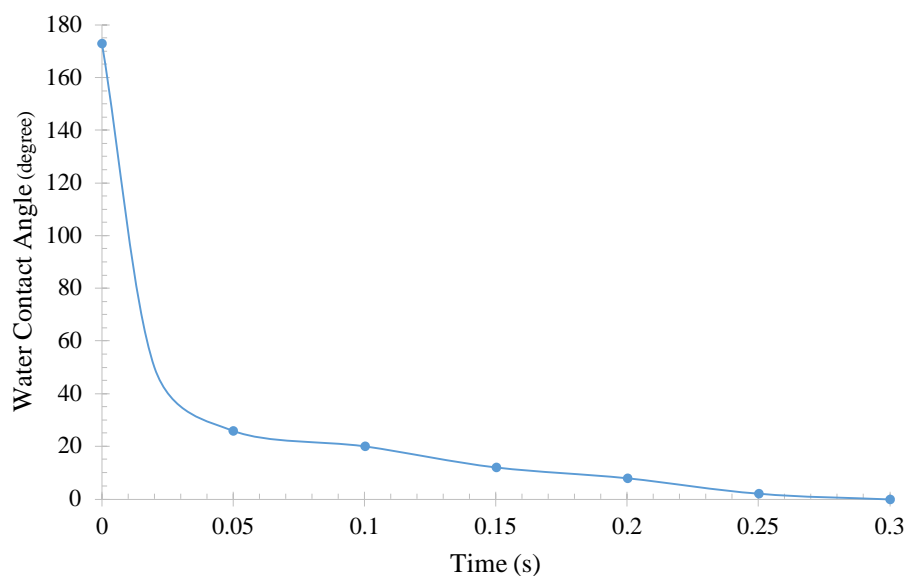

Figure 4. The superhydrophilicity characteristic of the MTiO$_2$–MXene composite membrane in oil–water separation.

Figure 5 illustrates the exceptional SH/SO properties of the WO$_3$–MXene composite membrane, showcasing its potential for oil–water separation applications. The presence of WO$_3$ in MXene nanochannels has been demonstrated to introduce superwetting properties with underwater oil contact angles. Moreover, previous studies have investigated the wettability of MXene−based membranes and have consistently shown that the addition of MXene material enhances the membrane's hydrophilicity. These compelling results strongly suggest that membranes based on MXene hold significant promise for oil–water separation due to their superwetting properties. The presented examples provide

compelling evidence of the SH/SO properties of the WO$_3$–MXene composite membrane, highlighting its potential for oil–water separation applications. The membrane's ability to repel oil while exhibiting exceptional hydrophilicity underscores its promise in addressing the challenges associated with efficient oil–water separation processes.
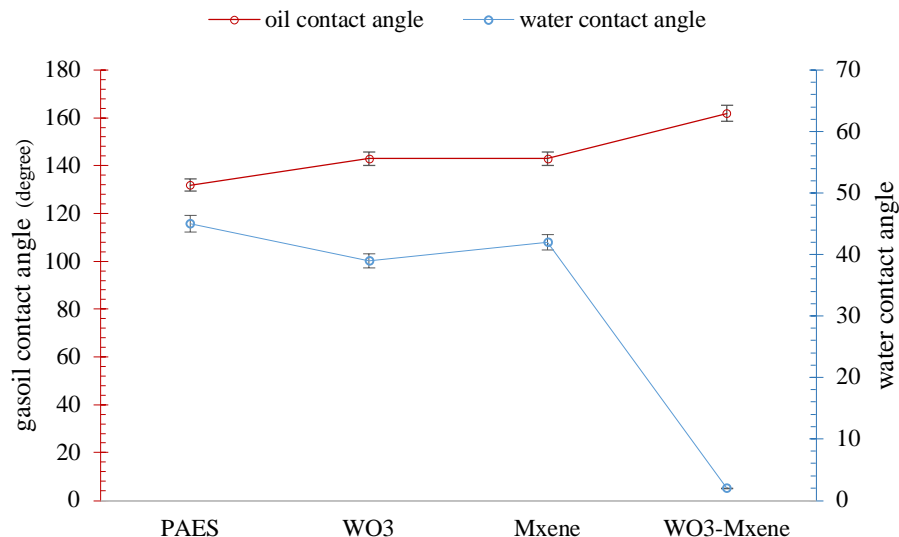

Figure 5. The gasoil contact angle and water contact angle of different membrane types including PAES, WO$_3$, MXene, and WO$_3$–MXene.

An experiment was conducted to test the fabricated membrane wettability with some types of ordinary oils, such as xylene, petrol, etc. The oil contact angles (OCAs) were not smaller than 140°, as shown in Figure 6. The composite membrane has been shown to be effective in the treatment of different light/heavy oils. Other investigations have explored the wettability of synthesized membranes for the removal of oil, including H and SH membranes with fluoropolymer coatings [39], and the wettability of photo-responsive membranes for oil treatment and photocatalytic pollutant degradation [40]. These studies have shown that membranes with wettability properties are suitable for separating oil and water.
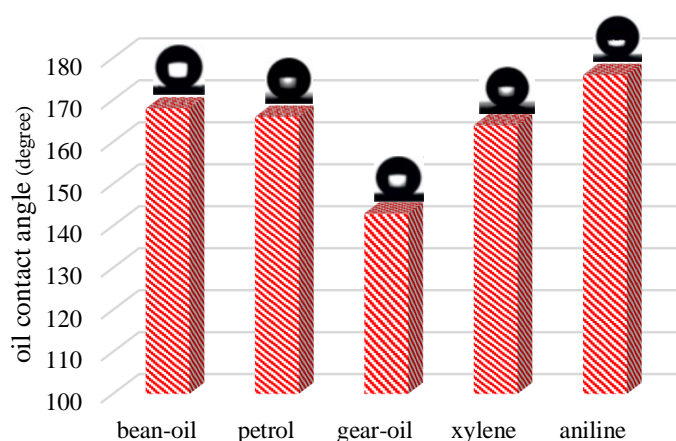

Figure 6. The oil contact angles (OCAs) of different types of oils, including bean oil, petrol, gear oil, xylene, and aniline on the fabricated WO$_3$–MXene membrane.

Figure 7 displays the surface and cross-section SEM images of the fabricated membranes. Figure 7a corresponds to the surface of the WO$_3$–MXene composite membrane, while Figure 7c corresponds to the cross-section SEM of the WO$_3$–MXene composite membrane. Figures 7b and 7d correspond to the surface and cross-section of the PAES membrane,

respectively. Upon careful examination of these results, it is evident that the pore size in the PAES membrane is smaller than that of the WO$_3$–MXene composite membrane, and it has less porosity. Therefore, it is predicted that the permeate flux of the PAES membrane is lower than that of the WO$_3$–MXene composite membrane.
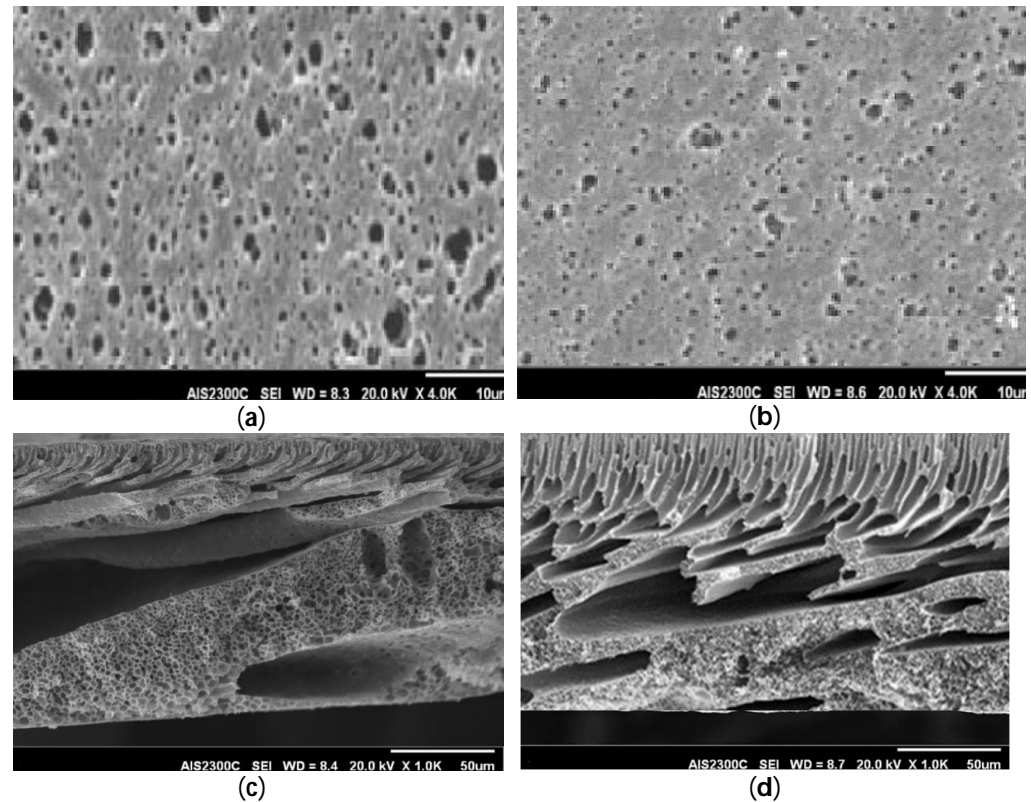

Figure 7. The surface and cross-section SEM images of the fabricated membranes; (**a**) the surface SEM of the WO$_3$–MXene composite membrane; (**b**) the surface SEM of the PAES membrane; (**c**) the cross-section SEM of the WO$_3$–MXene composite membrane; (**d**) the cross-section SEM of the PAES membrane.

The WO$_3$–MXene composite membrane demonstrated exceptional flux and oil–water separation efficiency, as illustrated in Figure 8. The incorporation of WO$_3$ into the MXene membrane resulted in a significant improvement in the treatment performance, achieving a 99.9% oil–water separation efficiency compared to the original 65.0%. Additionally, the permeate flux increased to 7.4 L/m^2.h from the previous 4.6 L/m^2.h. These impressive results highlight the potential of WO$_3$–MXene composite membranes for efficient gasoil–water emulsion separation and offer compelling evidence of the enhanced flux and oil–water separation efficiency of the WO$_3$–MXene composite membrane. The membrane's ability to achieve high separation efficiency and increased permeate flux makes it a promising candidate for various oil–water separation applications.

Our study demonstrated the exceptional performance of the WO$_3$–MXene fabricated membrane in treating oil-in-water emulsions, as depicted in Figure 9. The membrane exhibited outstanding treatment efficiency, with a performance higher than 99.4% for various types of oils, including bean oil, petrol, aniline, and xylene. Notably, the treatment efficiency for all cases, except for gear oil, exceeded 99.8%, with a flux greater than 7.2 L/m^2.h. Additionally, the membrane displayed a high water flux, with the lowest value recorded at 6.9 L/m^2.h for gear oil separation. These results underscore the potential of the composite membrane for efficient oil–water separation applications.
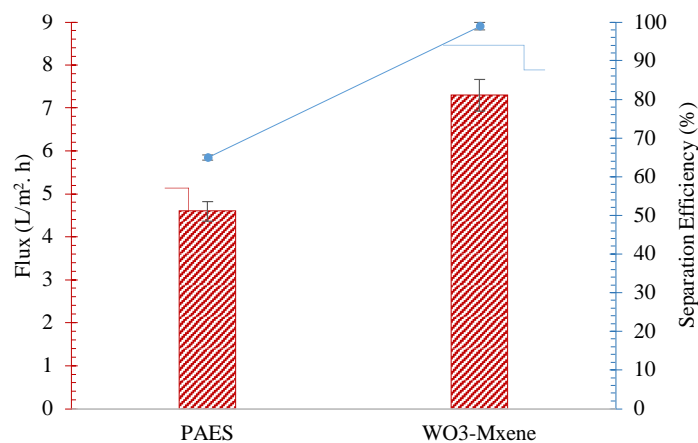
Figure 8. The flux and separation efficiency of WO$_3$-MXene composite membrane in separation of gasoil–water emulsions.
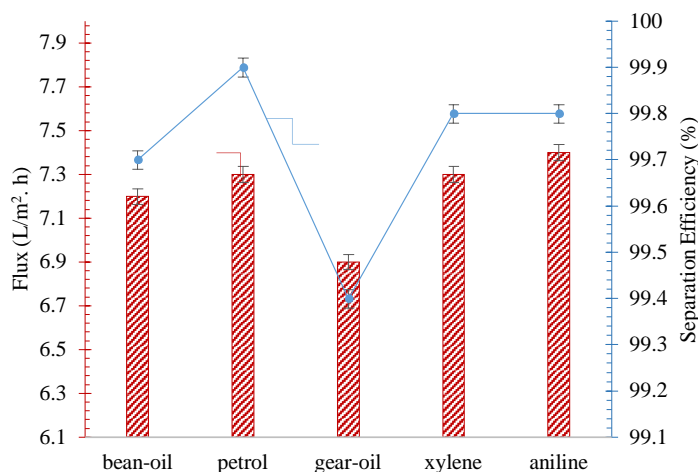

Figure 9. The flux and treatment efficiency of fabricated WO$_3$–MXene membrane in separation of different oil–water emulsions including bean oil, petrol, gear oil, aniline, and xylene.

In the study, the investigation of various cycles of treatment of gasoil-in-water revealed compelling results, as depicted in Figure 10. It was observed that the efficiency of the separation of the WO$_3$–MXene membrane decreased to 97% from 99.5%, and the permeate flux decreased to 6.3 L/m^2.h after six separation cycles. These findings underscore the importance of thoroughly explaining the results, as they highlight the evolving performance of the membrane over multiple process cycles. This nuanced understanding is crucial for comprehensively interpreting the implications of the study's outcomes and can provide valuable insights for further research and practical applications.

Oil droplets can block the channels of water transfer inside the fabricated membrane, which makes the fabricated membrane incapable of achieving high performance and rapid separation of oil from wastewater. This problem is common in membrane separation processes, and it can lead to membrane fouling.

The efficient treatment and flux of different oil emulsions in water were investigated in this study. Figures 11 and 12 show the results obtained for separation efficiency and flux, respectively. The highest drop in separation efficiency was observed when the bean oil emulsion in water was used as the feed. After six cycles, the separation efficiency decreased from 99.7% to 96.4%, while the flux of the permeate of the water decreased from 7.2 L/m^2.h to 6.8 L/m^2.h in the same six cycles. On the other hand, the treatment efficiency and flux for the xylene emulsion in water remained almost constant during these cycle tests. These findings suggest that the type of oil mixture used as the feed can significantly affect the separation efficiency and flux of the system.
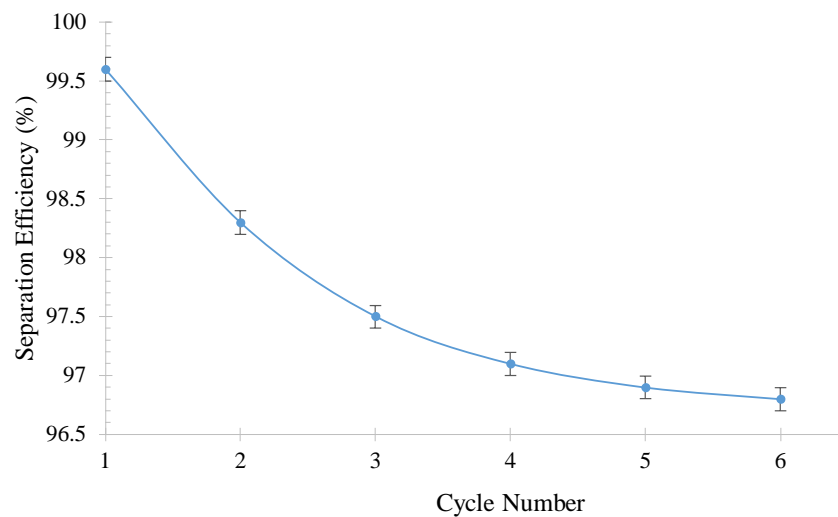
Figure 10. The treatment efficiency of WO$_3$–MXene membrane in separation of gasoil–water emulsions in different process cycles.
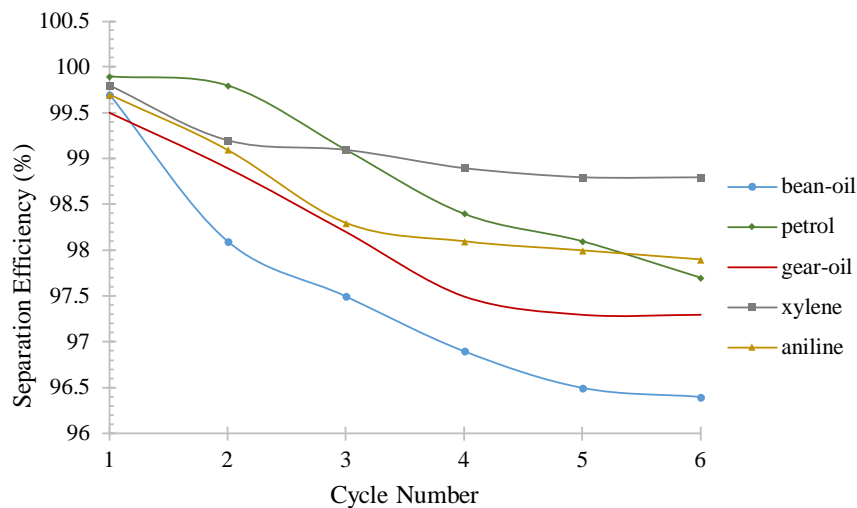

Figure 11. The treatment efficiency of WO$_3$–MXene membrane in separation of different oil–water emulsions in different process cycles including bean oil, petrol, gear oil, aniline, and xylene.
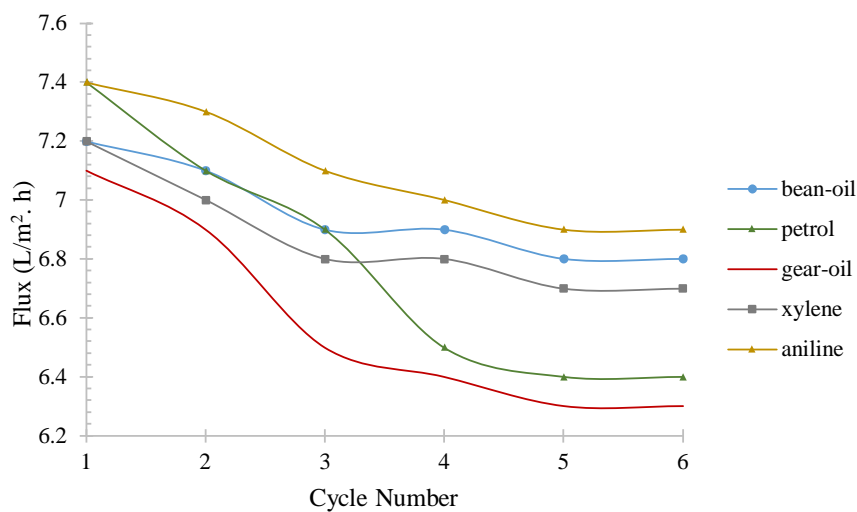

Figure 12. The permeated flux of WO$_3$–MXene composite membrane in separation of different oil–water emulsions in different process cycles including bean oil, petrol, gear oil, xylene, and aniline.

The fabricated composite membrane has exceptional self-cleaning and anti-fouling properties that are crucial in practical applications for separating oil–water mixtures. Table 1 shows the oil contact angle, separation efficiency, and flux of the fabricated membranes after different periods of irradiation in the range of 0 to 3 h. The results showed that the contaminated composite membrane's underwater SO property was restored (OCA > 155°) by being exposed to sunlight for different periods of irradiation.

Table 1. The oil contact angle, separation efficiency, and flux of the fabricated membranes after different periods of irradiation in the range of 0 to 3 h.

Irradiated Time (h)	Oil Contact Angle	Separation Efficiency (%)	Flux (L/m^2.h)
0	73 ± 3	96.31 ± 0.01	0.7 ± 0.1
0.25	155 ± 4	99.22 ± 0.01	5.1 ± 0.1
0.5	159 ± 4	99.40 ± 0.01	6.2 ± 0.1
1	161 ± 3	99.97 ± 0.01	6.3 ± 0.1
1.5	164 ± 5	99.97 ± 0.01	6.3 ± 0.1
2	163 ± 4	99.98 ± 0.01	6.4 ± 0.1
3	165 ± 3	99.98 ± 0.01	6.3 ± 0.1

The composite membrane showed a remarkable recovery time of only 0.25 h. Table 1 presents that the composite membrane with WO_3 or MXene could not regain its SH properties after 2 h of sunlight irradiation. As demonstrated in Table 1, the composite membrane's treatment efficiency and the water flux of the permeate recovered to 99.98% and 6.4 L/m^2.h, respectively.

In order to better demonstrate the effect of irradiation time on the performance of synthesized membranes, the changes in three parameters, including oil contact angle, separation efficiency, and permeate flux due to changes in irradiation time, are shown in Figure 13.

The remarkable improvements in the performance, self-cleaning, and anti-fouling properties of the composite membranes, as demonstrated in our study, highlight the immense potential of irradiation in enhancing membrane technology. With just 15 min of irradiation, we achieved significant results, including a 73% increase in the oil contact angle, a 3% enhancement in separation efficiency, and a seven-fold increase in permeate flux. This compelling evidence underscores the transformative impact of irradiation on membrane performance, even within a short timeframe. The degradation of contaminants in the fabricated membrane after sunlight irradiation can be attributed to the synergistic effects of WO_3 and MXene [41]. This process effectively addresses the issues of treatment efficiency and flux reduction caused by contamination. The use of electrochemical impedance spectroscopy (EIS) by Chen et al. [42] provided valuable insights into the transfer of electrons within the WO_3–MXene membrane. The extraordinary effects of irradiation on the performance, self-cleaning, and anti-fouling properties of composite membranes were vividly demonstrated in Figure 13.

Furthermore, the fabricated membrane interfering with both WO_3 and MXene showed an impedance value similar to the membrane interfering with WO_3 alone. This phenomenon can be related to the higher concentration of WO_3 compared to the concentration of MXene in the synthesized membranes. By adding MXene to the fabricated membranes, the resistance of the resulting membranes was significantly reduced due to the good electrical conductivity of MXene, and the fabricated WO_3–MXene membranes' impedance decreased due to the charge transfer of WO_3 after irradiation.

In conclusion, our findings showcase significant improvements in the performance, self-cleaning, and anti-fouling properties of composite membranes resulting from irradiation. Even within a short timeframe, irradiation has the potential to revolutionize membrane technology and pave the way for more efficient and sustainable water treatment solutions.
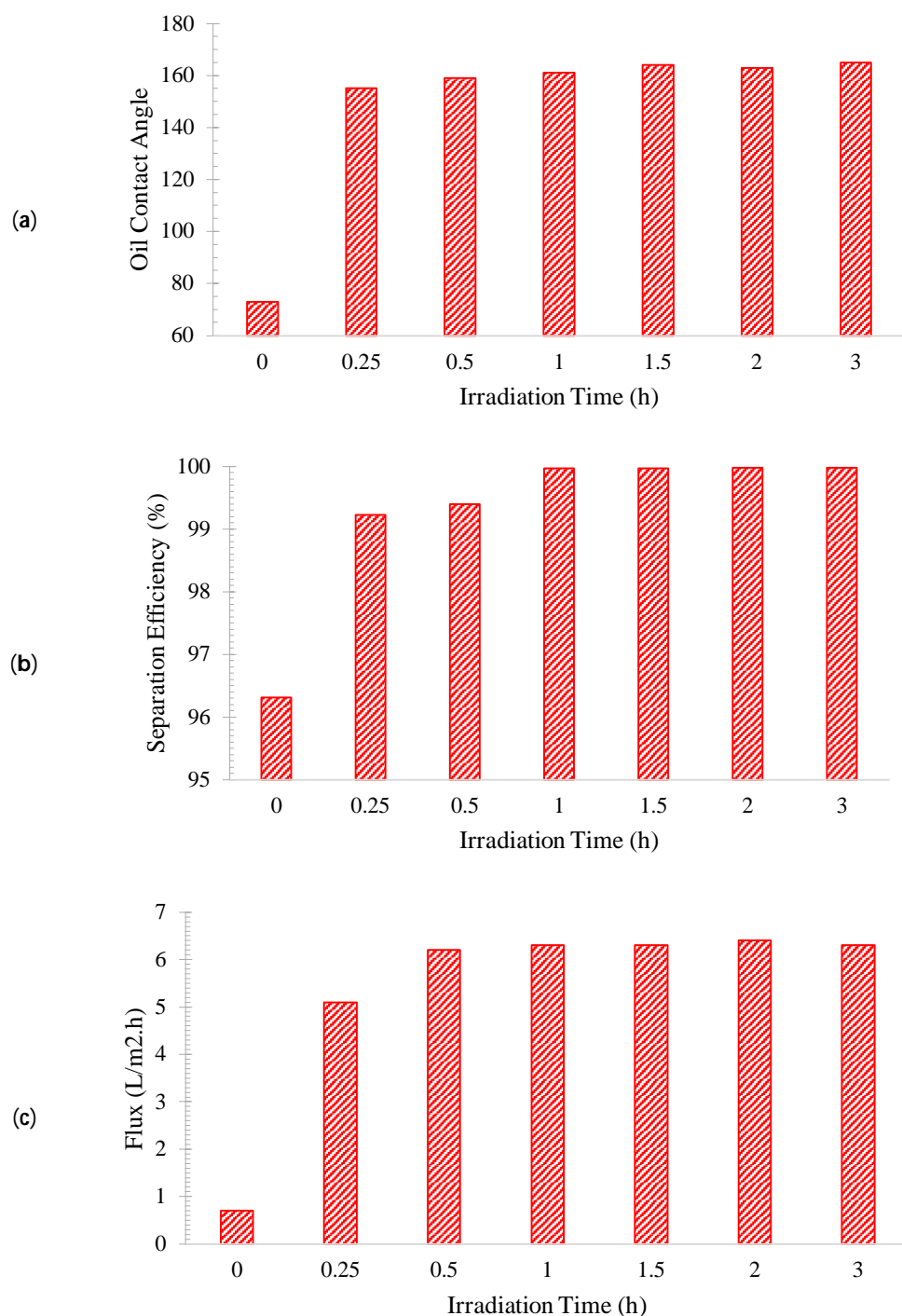
Figure 13. The effect of irradiation time on the performance of synthesized membranes: (**a**) oil contact angle, (**b**) separation efficiency, and (**c**) permeate flux.

4. Conclusions

This study presents a highly innovative approach for efficient oil–water separation using a tungsten (VI) oxide (WO$_3$)/MXene composite membrane based on poly (arylene ether sulfone) (PAES). With superoleophobic (SO) and superhydrophilic (SH) properties, the membrane effectively treats oil-in-water emulsions. Furthermore, brief sunlight exposure triggers the photodegradation of contaminants, granting the membrane self-cleaning and anti-fouling properties. The study demonstrates that the composite membrane has a remarkable recovery time of only 15 min, resulting in a 73% increase in the oil contact

angle, a 3% enhancement in separation efficiency, and a seven-fold increase in permeate flux. The influence of WO_3 and MXene on the composite membrane effectively degrades contaminants into non-polluting substances upon sunlight irradiation. This innovative work addresses the challenges of treatment efficiency and the reduction in water flux caused by contamination. The results offer promising solutions to water pollution challenges and hold potential for practical applications from self-cleaning and anti-fouling points of view. The study demonstrates the potential of composite membranes in water treatment and provides a novel direction for research in the future in the field of membrane separation. The findings highlight the importance of developing efficient oil–water separation methods to address the rising global crisis of water pollution. Overall, the results of this study provide strong evidence that the WO_3/MXene composite membrane is a highly effective and promising solution for oil–water separation and water treatment.

Author Contributions: Conceptualization, A.A., H.O., M.B., M.K.A., M.S. and S.S.S.; data curation, M.B.; formal analysis, A.A., H.O. and M.K.A.; funding acquisition, M.S.; investigation, A.A., M.B. and S.S.S.; project administration, S.S.S.; resources, A.A., M.K.A., M.S. and S.S.S.; supervision, M.S.; validation, H.O. and M.S.; visualization, H.O.; writing—original draft, A.A., H.O., M.B., M.K.A. and S.S.S.; writing—review and editing, M.S. All authors have read and agreed to the published version of the manuscript.

Data Availability Statement: The data that support the findings of this study are available on request from the corresponding author.

Conflicts of Interest: Author Miklas Scholz was employed by the company Kunststoff-Technik Adams. The remaining authors declare that the research was conducted in the absence of any commercial or financial relationships that could be construed as a potential conflict of interest.

References

1. Tong, S.; Bambrick, H.; Beggs, P.J.; Chen, L.; Hu, Y.; Ma, W.; Steffen, W.; Tan, J. Current and Future Threats to Human Health in the Anthropocene. *Environ. Int.* **2022**, *158*, 106892. [CrossRef]
2. Hamta, A.; Mohammadi, A.; Dehghani, M.R.; Feyzi, F. Liquid–Liquid Equilibrium and Thermodynamic Modeling of Aqueous Two-Phase System Containing Polypropylene Glycol and $NaClO_4$ at T = (288.15 and 298.15) K. *J. Solut. Chem.* **2018**, *47*, 1–25. [CrossRef]
3. Wagner, M.; Lin, K.-Y.A.; Oh, W.-D.; Lisak, G. Metal-Organic Frameworks for Pesticidal Persistent Organic Pollutants Detection and Adsorption–A Mini Review. *J. Hazard. Mater.* **2021**, *413*, 125325. [CrossRef] [PubMed]
4. Sadek, A.H.; Fahmy, O.M.; Nasr, M.; Mostafa, M.K. Predicting Cu(II) Adsorption from Aqueous Solutions onto Nano Zero-Valent Aluminum (NZVAl) by Machine Learning and Artificial Intelligence Techniques. *Sustainability* **2023**, *15*, 2081. [CrossRef]
5. Hamta, A.; Dehghani, M.R. Application of Polyethylene Glycol Based Aqueous Two-Phase Systems for Extraction of Heavy Metals. *J. Mol. Liq.* **2017**, *231*, 20–24. [CrossRef]
6. Assegide, E.; Alamirew, T.; Dile, Y.T.; Bayabil, H.; Tessema, B.; Zeleke, G. A Synthesis of Surface Water Quality in Awash Basin, Ethiopia. *Front. Water* **2022**, *4*, 782124. [CrossRef]
7. Nawaz, S.; Tabassum, A.; Muslim, S.; Nasreen, T.; Baradoke, A.; Kim, T.; Boczkaj, G.; Jesionowski, T.; Bilal, M. Effective Assessment of Biopolymer-Based Multifunctional Sorbents for the Remediation of Environmentally Hazardous Contaminants from Aqueous Solutions. *Chemosphere* **2023**, *329*, 138552. [CrossRef] [PubMed]
8. Fawzy, M.; Nasr, M.; Abdel-Gaber, A.; Fadly, S. Biosorption of Cr(VI) from Aqueous Solution Using Agricultural Wastes, with Artificial Intelligence Approach. *Sep. Sci. Technol.* **2016**, *51*, 416–426. [CrossRef]
9. Hamta, A.; Ashtiani, F.Z.; Karimi, M.; Moayedfard, S. Asymmetric Block Copolymer Membrane Fabrication Mechanism through Self-Assembly and Non-Solvent Induced Phase Separation (SNIPS) Process. *Sci. Rep.* **2022**, *12*, 771. [CrossRef]
10. Xiao, Y.; Tang, Z.; Xu, X.; Zhang, X.; Shi, Y. A Deep Koopman Operator-based Modelling Approach for Long-term Prediction of Dynamics with Pixel-level Measurements. *CAAI Trans. Intell. Technol.* **2024**, *9*, 178–196. [CrossRef]
11. Hamta, A.; Zokaee Ashtiani, F.; Karimi, M.; Safikhani, A. Manipulating of Polyacrylonitrile Membrane Porosity via SiO_2 and TiO_2 Nanoparticles: Thermodynamic and Experimental Point of View. *Polym. Adv. Technol.* **2020**, *32*, 872–885. [CrossRef]

12. Kong, Q.; Wang, W.; Zhang, D.; Zhang, W. Two Kinds of Average Approximation Accuracy. *CAAI Trans. Intell. Technol.* **2024**, *9*, 481–490. [CrossRef]

13. Hamta, A.; Ashtiani, F.Z.; Karimi, M.; Sadeghi, Y.; MoayedFard, S.; Ghorabi, S. Copolymer Membrane Fabrication for Highly Efficient Oil-in-Water Emulsion Separation. *Chem. Eng. Technol.* **2021**, *44*, 1321–1326. [CrossRef]

14. Zheng, G.; Chen, W.; Qian, Q.; Kumar, A.; Sun, W.; Zhou, Y. TCM in Milling Processes Based on Attention Mechanism-Combined Long Short-Term Memory Using a Sound Sensor under Different Working Conditions. *Int. J. Hydromechatron.* **2022**, *5*, 243–259. [CrossRef]

15. Li, J.; Shang, H.; Yan, J.; Qiao, M.; Yu, J.; Zhu, D.; He, C. Micro Drilling of PMMA with Double-Pulse Femtosecond Laser. *Int. J. Hydromechatron.* **2023**, *6*, 34–44. [CrossRef]

16. Hamta, A.; Dehghani, M.R.; Gholami, M. Novel Experimental Data on Aqueous Two–Phase System Containing PEG–6000 and Na_2CO_3 at T = (293.15, 303.15 and 313.15) K. *J. Mol. Liq.* **2017**, *241*, 144–149. [CrossRef]

17. Solyali, D.; Mollaei, A. A Simulation Model Based on Experimental Data to Determine the Optimal Tilt Angle for a Fixed Photovoltaic Panel. *Arch. Adv. Eng. Sci.* **2023**, 1–11. [CrossRef]

18. Sun, Y.; Ma, P.; Dai, J.; Li, D. A Cloud Bayesian Network Approach to Situation Assessment of Scouting Underwater Targets with Fixed-wing Patrol Aircraft. *CAAI Trans. Intell. Technol.* **2023**, *8*, 532–545. [CrossRef]

19. Koo, D.C.H.; Tan, N.N.; Ng, Q.H.; Rahim, S.K.E.A.; Low, S.C.; Yeo, R.Y.Z. Integrating Advanced Keggin-Structure Polyoxometalate into Polymeric Membrane to Enhance Photocatalytic Self-Cleaning and Antifouling Functionalities. *Korean J. Chem. Eng.* **2022**, *39*, 1045–1052. [CrossRef]

20. Li, C.; Sun, T.; Yi, G.; Zhang, D.; Zhang, Y.; Lin, X.; Liu, J.; Shi, Z.; Lin, Q. Fabrication of a Ag/CNQDs/g-C3N4-PVDF Photocatalytic Composite Membrane with Excellent Photocatalytic and Self-Cleaning Properties. *J. Environ. Chem. Eng.* **2022**, *10*, 108488. [CrossRef]

21. Asmael, M.; Memarzadeh, A. A Review on Recent Achievements and Challenges in Electrochemical Machining of Tungsten Carbide. *Arch. Adv. Eng. Sci.* **2024**, *2*, 1–23. [CrossRef]

22. Kanakaraju, D.; Chandrasekaran, A. Recent Advances in TiO_2/ZnS-Based Binary and Ternary Photocatalysts for the Degradation of Organic Pollutants. *Sci. Total Environ.* **2023**, *868*, 161525. [CrossRef]

23. Liu, Y.; Zhao, Y.; Lumkes, J.; Zhang, S.; Yu, K.; Chen, L. Parameter Optimisation Design of Mixing and Distributing System of Vertical Biaxial Bladed Mixer. *Int. J. Hydromechatron.* **2023**, *6*, 133–158. [CrossRef]

24. Soni, V.; Singh, P.; Quang, H.H.P.; Khan, A.A.P.; Bajpai, A.; Van Le, Q.; Thakur, V.K.; Thakur, S.; Nguyen, V.-H.; Raizada, P. Emerging Architecture Titanium Carbide (Ti_3C_2Tx) MXene Based Photocatalyst toward Degradation of Hazardous Pollutants: Recent Progress and Perspectives. *Chemosphere* **2022**, *293*, 133541. [CrossRef] [PubMed]

25. Shekoofa, O.; Wang, J.; Li, D. Fabrication of N-Type Nanocrystalline Silicon Thin-Film by Magnetron Sputtering and Antimony Induced Crystallization. *Arch. Adv. Eng. Sci.* **2023**, *2*, 71–78. [CrossRef]

26. Li, Z.; Yin, L.; Jiang, S.; Chen, L.; Sang, S.; Zhang, H. A Photocatalytic Degradation Self-Cleaning Composite Membrane for Oil-Water Separation Inspired by Light-Trapping Effect of Moth-Eye. *J. Memb. Sci.* **2023**, *669*, 121337. [CrossRef]

27. Lin, Q.; Zeng, G.; Yan, G.; Luo, J.; Cheng, X.; Zhao, Z.; Li, H. Self-Cleaning Photocatalytic MXene Composite Membrane for Synergistically Enhanced Water Treatment: Oil/Water Separation and Dyes Removal. *Chem. Eng. J.* **2022**, *427*, 131668. [CrossRef]

28. He, H.; Li, Z.; Ouyang, L.; Liang, Y.; Yuan, S. Hierarchical WO_3@ Cu $(OH)_2$ Nanorod Arrays Grown on Copper Mesh with Superwetting and Self-Cleaning Properties for High-Performance Oil/Water Separation. *J. Alloys Compd.* **2021**, *855*, 157421. [CrossRef]

29. Kusworo, T.D.; Yulfarida, M.; Kumoro, A.C.; Sumardiono, S.; Djaeni, M.; Kurniawan, T.A.; Othman, M.H.D.; Budiyono, B. A Highly Durable and Hydrophilic PVDF-MoS_2/WO_3-PVA Membrane with Visible Light Driven Self-Cleaning Performance for Pollutant-Burdened Natural Rubber Wastewater Treatment. *J. Environ. Chem. Eng.* **2023**, *11*, 109583. [CrossRef]

30. Harrison, W.L. Synthesis and Characterization of Sulfonated Poly (Arylene Ether Sulfone) Copolymers via Direct Copolymerization: Candidates for Proton Exchange Membrane Fuel Cells. Ph.D. Dissertation, Virginia Polytechnic Institute and State University, Blacksburg, VA, USA, 2002.

31. Najafi-Ashtiani, H.; Bahari, A.; Gholipour, S.; Hoseinzadeh, S. Structural, Optical and Electrical Properties of WO_3–Ag Nanocomposites for the Electro-Optical Devices. *Appl. Phys. A* **2018**, *124*, 24. [CrossRef]

32. Pandurangarao, K.; Kumar, V.R. Preparation and Characterization of Nanocrystalline Tungsten Oxide Thin Films for Electrochromic Devices: Effect of Deposition Parameters. *Mater. Today Proc.* **2019**, *19*, 2596–2603. [CrossRef]

33. Kanan, S.M.; Lu, Z.; Cox, J.K.; Bernhardt, G.; Tripp, C.P. Identification of Surface Sites on Monoclinic WO_3 Powders by Infrared Spectroscopy. *Langmuir* **2002**, *18*, 1707–1712. [CrossRef]

34. Du, Q.; Men, Q.; Li, R.; Cheng, Y.; Zhao, B.; Che, R. Electrostatic Adsorption Enables Layer Stacking Thickness-Dependent Hollow $Ti_3C_2T_x$ MXene Bowls for Superior Electromagnetic Wave Absorption. *Small* **2022**, *18*, 2203609. [CrossRef]

35. Qian, J.; Wang, C.; Zhang, X.; Hu, J.; Zhao, X.; Li, J.; Ren, Q. Quaternary Ammonium-Functionalized Crosslinked Poly (Aryl Ether Sulfone) s Anion Exchange Membranes with Enhanced Alkaline Stability for Water Electrolysis. *J. Memb. Sci.* **2023**, *685*, 121946. [CrossRef]

36. Ling, M.; Yu, K.; Wang, J.; Wang, H.; Nie, H.; Wang, Z.; Zhou, G. Synthesis and Pyrolysis Mechanism of Phenolphthalein Poly (Aryl Ether Sulfone) Containing Isopropyl Groups. *Thermochim. Acta* **2022**, *714*, 179253. [CrossRef]

37. Huang, Y.; Lu, Q.; Wu, D.; Jiang, Y.; Liu, Z.; Chen, B.; Zhu, M.; Schmidt, O.G. Flexible MXene Films for Batteries and Beyond. *Carbon Energy* **2022**, *4*, 598–620. [CrossRef]

38. Iakunkov, A.; Nordenström, A.; Boulanger, N.; Hennig, C.; Baburin, I.; Talyzin, A.V. Temperature-Dependent Swelling Transitions in MXene Ti$_3$C$_2$Tx. *Nanoscale* **2022**, *14*, 10940–10949. [CrossRef] [PubMed]

39. Melnik, A.; Bogoslovtseva, A.; Petrova, A.; Safonov, A.; Markides, C.N. Oil–Water Separation on Hydrophobic and Superhydrophobic Membranes Made of Stainless Steel Meshes with Fluoropolymer Coatings. *Water* **2023**, *15*, 1346. [CrossRef]

40. Baig, U.; Dastageer, M.A. Fabrication of Photo-Responsive Mesh Membrane with Surface-Engineered Wettability for Oil–Water Separation and Photocatalytic Degradation of Organic Pollutants. *Membranes* **2023**, *13*, 302. [CrossRef]

41. Havelka, O.; Yalcinkaya, F.; Wacławek, S.; Padil, V.V.T.; Amendola, V.; Cernik, M.; Torres-Mendieta, R. Sustainable and Scalable Development of PVDF-OH Ag/TiOx Nanocomposites for Simultaneous Oil/Water Separation and Pollutant Degradation. *Environ. Sci. Nano* **2023**, *10*, 2359–2373. [CrossRef]

42. Chen, W.; Liu, M.; Ding, M.; Zhang, L.; Dai, S. Advanced Thin-Film Composite Polyamide Membrane for Precise Trace Short-Chain PFAS Sieving: Solution, Environment and Fouling Effects. *Process Saf. Environ. Prot.* **2023**, *169*, 493–503. [CrossRef]